Experimental Neurology **168,** 63–77 (2001)
doi:10.1006/exnr.2000.7554, available online at http://www.idealibrary.com on IDEAL®

Microglia, Astrocytes, and Macrophages React Differentially to Central and Peripheral Lesions in the Developing and Mature Rat Whisker-to-Barrel Pathway: A Study Using Immunohistochemistry for Lipocortin1, Phosphotyrosine, S100β, and Mannose Receptors

Peter Melzer,[1] Valentina Savchenko, and James A. McKanna

Department of Cell Biology, Vanderbilt University School of Medicine, Nashville, Tennessee 37232

Received January 3, 2000; accepted August 25, 2000

Adult and neonatal rats were subjected to transection of the left infraorbital nerve or ablation of the left parietal cortex. The ensuing glial reaction in the whisker-to-barrel pathway was studied with immunohistochemistry for Lipocortin1- (LC1+), phosphotyrosine- (PY+), S100β- (S100β+), and mannose receptor- (MR+) immunoreactive microglia, astrocytes, and macrophages. Four days after infraorbital nerve transection in adult rats, LC1+ and PY+ microglia were prominently increased in the trigeminal sensory brain-stem nuclei on the deafferented side compared with the intact side. Changes were negligible at the second synapse of the pathway, i.e., the thalamic ventroposterior medial nucleus. Cortical ablation in adults led to an increase in microglia in the ipsilateral ventroposterior medial nucleus that reciprocally connects with the ablated cortex. Moreover, microglial reactions occurred in the contralateral trigeminal sensory brainstem nuclei in which corticofugal projections from the ablated cortex terminate. S100β+ astrocytes, in contrast, appeared unaltered after both types of lesion in adults. In neonates, LC1+, PY+, and S100β+ cells did not have the adult morphology of microglia or astrocytes. Four days after nerve transection, LC1+ and PY+ cells were sparse and remained unchanged. In contrast, S100β+ cells substantially increased in the deafferented trigeminal brain-stem nuclei. Four days after cortical ablation in neonates, LC1+, PY+, and S100β+ cells had accumulated in the deprived thalamus. In contrast to adults, many of these cells were MR+ macrophages. In the deprived brain-stem, only S100β+ cells increased and none were macrophages. Therefore, macrophages do not appear to stem from microglia, and neonatal LC1+, PY+, and S100β+ cells may possess functions different from those in adults.

Key Words: **infraorbital nerve transection; cortical ablation; glial reaction; whiskers; barrels; rat.**

INTRODUCTION

Microglia appear to play a crucial role in cerebral homeostasis. They are resident in the parenchyma of the brain where they are evenly dispersed. Their density reaches about 1–1.5 cells per 100 μm^2 in gray matter of the adult rat (31). After brain damage, however, their population density increases at the site of neural injury. Forel (17) may have been the first to observe microglia accumulating in the guinea pig facial nerve tract and nucleus after rhizotomy (Fig. 2A, top inset). The origin of these cells, which he termed "Spinnenzellen" (spider cells), remained obscure to him though he speculated that some spider cells might have been glia. Eventually Penfield (39) observed that these cells, which he named "microglia," phagocytose cellular debris after brain damage. Furthermore, in response to neural injury microglia were shown to transform from a *resting* into an *activated* state (13) and to proliferate mitotically (7, 27). Since facial nerve transection led to a microglial reaction without breaching the blood–brain barrier, the cells of origin for the microglial proliferation were assumed to be resident in the brain (43). In harmony with this, transection of the infraorbital branch of the trigeminal nerve does not disrupt the blood–brain barrier and results in a prominent glial reaction in the trigeminal sensory brain-stem nuclei in adult rats (36).

As the nuclei of termination of the primary afferents of the whisker-to-barrel pathway, the trigeminal sensory brain-stem nuclei connect receptors in whisker follicles via the contralateral thalamic ventroposterior medial nucleus with a subdivision of the primary somatosensory cortex. This subdivision is composed of discrete cytoarchitectonic units, named "barrels," that represent the whiskers topologically (47). Similar so-

[1] To whom correspondence should be addressed.

0014-4886/01 $35.00

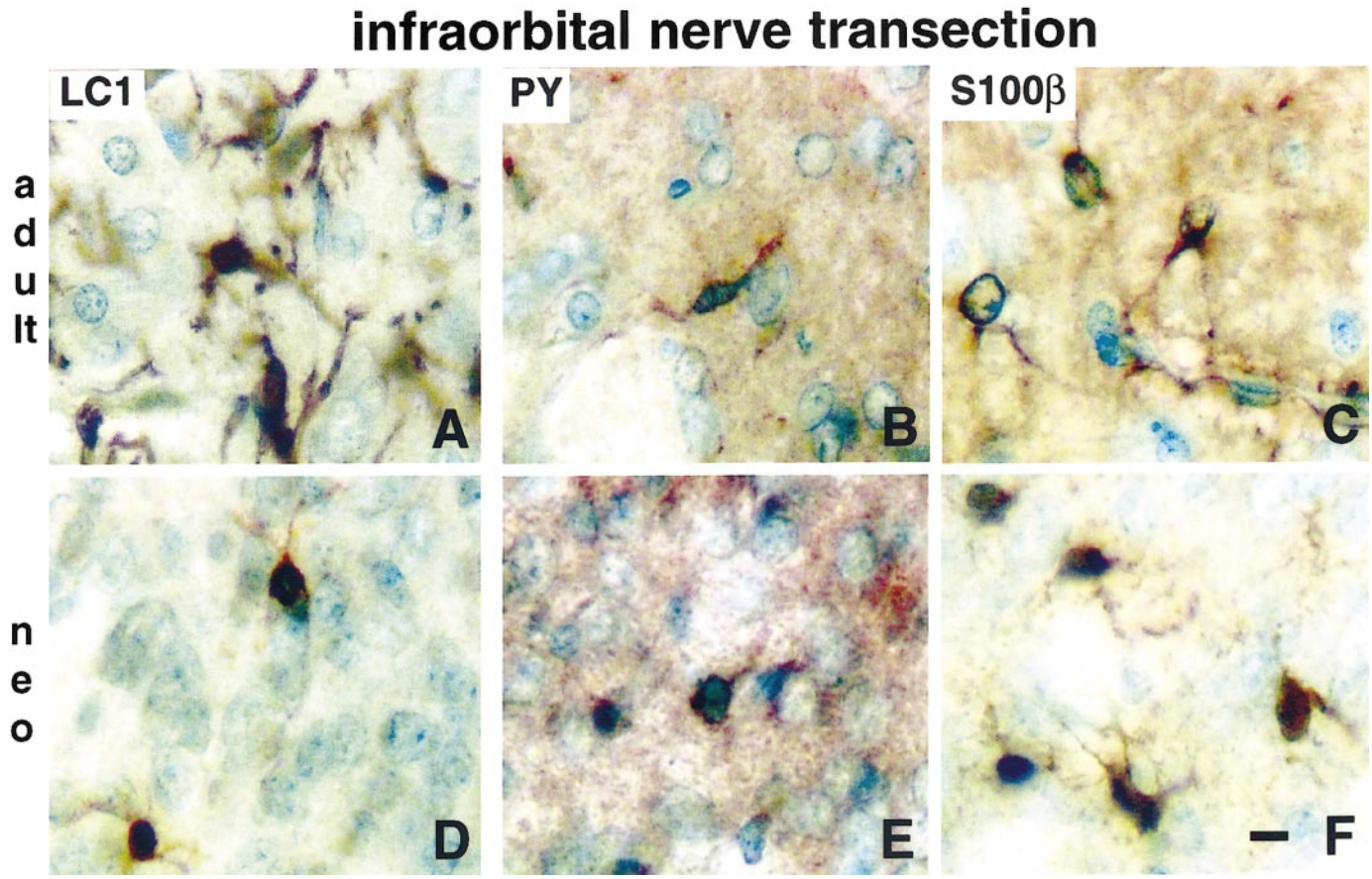

FIG. 1. Cellular responses 4 days after infraorbital nerve transection in adults (A–C) and neonates (D–F). Adjacent 10-μm-thick transverse sections through deafferented trigeminal sensory brain-stem subnucleus caudalis were processed with immunohistochemistry for LC1 (A and D), PY (B and E), and S100β (C and F) and stained with toluidine blue. In adults, most LC1+ cells exhibited the typical features of microglia in advanced activated state, i.e., polymorphic somata with nuclei smaller than 10 μm and cytoplasmic processes that were thickened proximally and had multiple ramifications (A). PY+ cells had polymorphic somata and processes and were similar in appearance to any of the small LC1+ microglia (B). S100β+ cells possessed attributes typical of astrocytes, i.e., large round nuclei surrounded by a thin rim of cytoplasm and processes with few branches (C). In neonates, LC1+ cells were rare. They had polymorphic somata and cytoplasmic processes with few branches (D). PY+ cells were pleomorphic and had short, unbranched processes (E). S100β+ cells resembled LC1+ cells in appearance, but were more numerous (F). Orientation: dorsal is up; the animal's left side is right. The bar in F represents 10 μm.

matotopic morphological whisker representations have been found at the subcortical synaptic relays (4, 30, 44). After the transection of the infraorbital nerve at birth, the morphological whisker representations in the trigeminal sensory brain-stem nuclei vanish (10) and the terminal fields of primary afferents enlarge (41), entailing pruning and elongation of their terminations (42). Within 4 days the reorganization of terminations has reached the barrel cortex (8) and cellular debris has been produced along the entire ascending pathway. Scavenging for cellular debris has been the major role attributed to microglia (13). However, differentiated microglia are rare in neonates (31, 32) and there is evidence that transient macrophages play the role of scavengers in the developing brain (37). The aim of the present study was to investigate the nonneuronal cells that participate in reorganization of the whisker-to-barrel pathway in adults and neonates after infraorbital nerve transection and to explore differences in the glial reaction when the blood–brain barrier is breached by comparing nerve transection with cortical ablation. Immunohistochemistry for Lipocortin1, phosphotyrosine, S100β, and mannose receptors was used to identify microglia, activated microglia, astrocytes, and macrophages, respectively (24, 29, 31).

MATERIAL AND METHODS

All experiments were carried out in accordance with the NIH guide for the care and use of laboratory animals. Adult and newborn Long–Evans rats of either sex were used in this study. The animals were housed in 14-h/10-h light/dark cycles with food and water *ad libitum*.

Lesions in adults. Adult male and female Long–Evans rats (ca. 400 g bw) were subjected to nerve

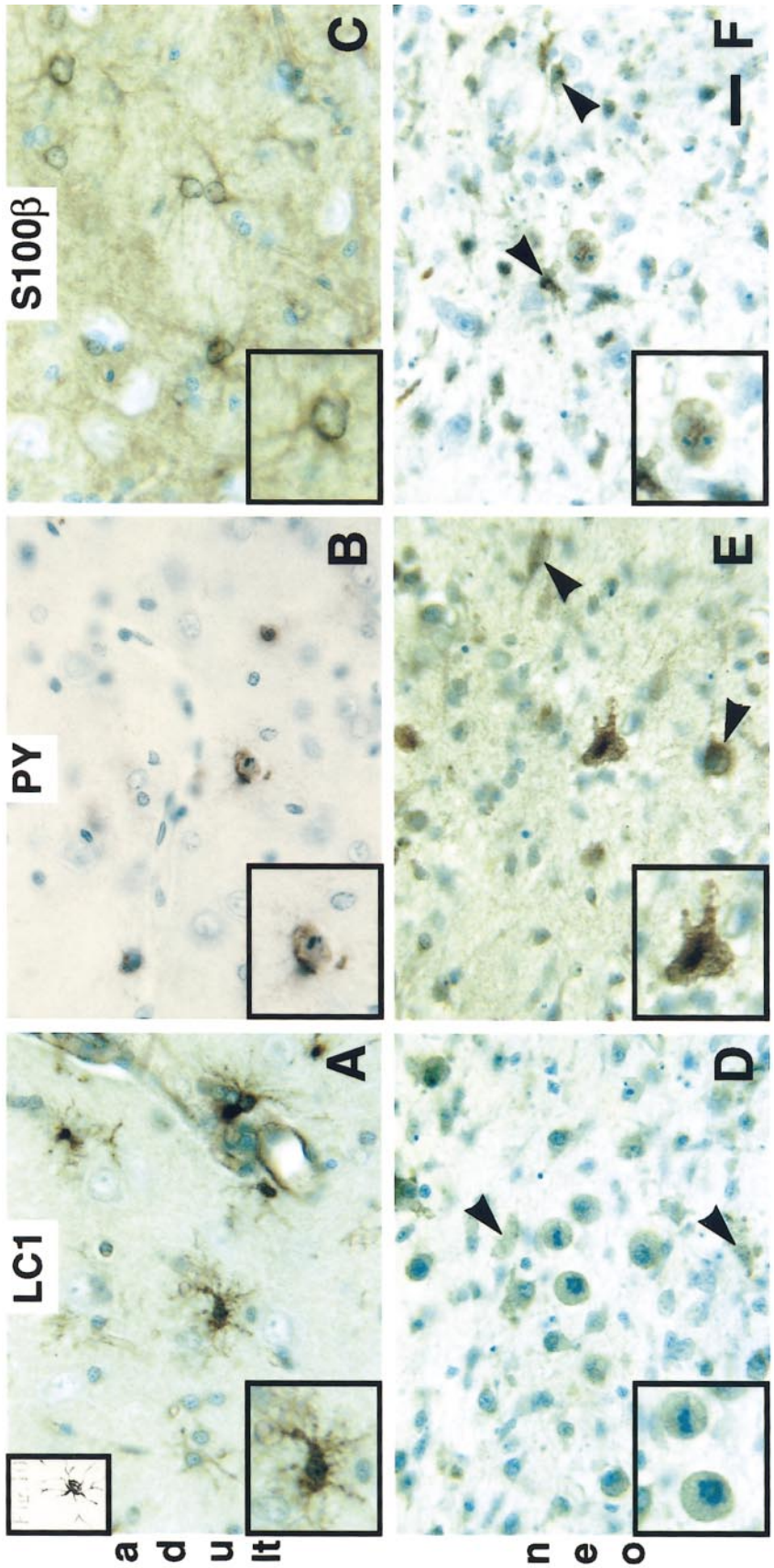

FIG. 2. Cellular responses in the deprived ventroposterior medial nucleus 4 days after cortical ablation in adults (A–C) and neonates (D–F). Adjacent 10-μm-thick coronal sections through the diencephalon were processed with immunohistochemistry for LC1 (A and D), PY (B and E), and S100β (C and F) and stained with toluidine blue. The insets at the bottom left corners show further enlargements of the most conspicuous cell type labeled with the respective marker. In adults, the LC1+ cells that were most frequently observed were activated microglia (A). There is a great resemblance between these cells and Forel's (17) spider cells (compare inset at bottom with inset at top in A). PY+ cells resembled small microglia (B). S100β+ cells had the typical morphology of astrocytes (C). In neonates, we observed LC1+ cells (D) that were either spherical (ca. 20 μm in diameter) and bare of cytoplasmic processes (enlarged in inset) or ovoid with processes (arrowhead). A few spherical cells exhibited mitotic figures. The most conspicuous PY+ cell type was pleomorphic with pseudopodia (E; arrowhead and enlarged in inset). S100β+ cells (F) were either spherical and arborless (enlarged in inset) or polymorphic with processes (arrowheads). The spherical cells contained granules stained with toluidine blue. Orientation: dorsal is up; the animal's left side is right. The bar in F represents 20 μm (15 μm in the insets).

transection or cortical ablation under pentobarbital anesthesia (40 mg/kg ip). Lidocaine was applied to the wounds' edge.

In four rats, the left infraorbital nerve was exposed at the infraorbital foramen and transected, and the wound was sutured. After 4 days, the rats were euthanized by an intraperitoneal overdose of pentobarbital. Eight rats underwent cortical ablations. The skin was incised along the central fissure. The left parietal bone was exposed and removed after circumferential incision with a dental burr. The parietal cortex was aspirated. The bone was repositioned and cemented with polycarboxylate cement, and the wound was sutured. After recovery the rats were returned to their cages and held under the conditions described above for 2, 4, 6, and 8 days, when they were euthanized by barbiturate overdose.

Lesions in neonates. Pregnant females were checked for offspring twice daily. On the day of birth, four pups from one litter and three pups from a second litter were subjected to unilateral infraorbital nerve transection. Under pentobarbital anesthesia (30 mg/kg ip) supported by hypothermia, the skin over the infraorbital foramen on the left side was incised and the infraorbital nerve was exposed and transected. Any bleeding was arrested with gel foam. In four neonates from two litters (two from each), the left parietal bone was exposed under anesthesia with a longitudinal incision of the skin above the central fissure. The skull was incised over the left cortical hemisphere lateral to the sagittal sinus, caudal to the bregma, and rostral to the fissura lambdoidea to create a bone flap and the parietal cortex was aspirated through the opening. The flap was reaffixed to the skull with anhydrous polycarboxylate cement (Tylkol-Plus; Dentsply International, Inc., Milford, DE) and the wound was sutured. After both types of lesion, Lidocaine was applied to the wounds' edges to further alleviate pain; the pups were warmed up, wiped with peanut oil, and returned to their mothers in the animal facility. Four days after either lesion the pups were euthanized with an intraperitoneal injection of pentobarbital (80 mg/kg).

Immunohistochemistry. After pentobarbital injection, the animals were injected with heparin (1000 units/kg ip) and transcardially perfused with saline (50 ml for adults; 5 ml for pups), containing heparin (1000 units) and 0.01% $NaNO_2$, followed by either 150 (adults) or 15 ml (pups) of glutaraldehyde (2.5%), periodate sodium (10 mM), acetic acid (1.0%), phosphate-buffered saline (0.9% NaCl in 40 mM buffer) (33). The brains were removed, postfixed, and embedded in paraffin. Alternate series of 10-μm-thick coronal sections were obtained. After deparaffinization, the sections were immunostained using polyclonal rabbit antisera raised against human placental Lipocortin1 [1:8000 (31)], S100β [1:8000 (32)], tyrosine-phosphorylated proteins (1:1000; No. 61-5800; Zymed Laboratories, Inc., South San Francisco, CA), or macrophage mannose receptors [1:500 (29)] and counterstained with toluidine blue.

Data assessment. The preparations were analyzed under a microscope (Ortholux; Leitz, Wetzlar, FRG) for differences in morphology and population density of immunoreactive cells. Limits for size and thresholds for staining intensity were set empirically in digitized video images by the investigator to exclude partially cut cell bodies and processes; the cellular profiles were measured and mapped (Bioquant; R&M Biometrics, Inc., Nashville, TN). Trigeminal brain-stem subnucleus caudalis, subnucleus interpolaris, and nucleus principalis as well as the thalamic ventroposterior medial nucleus were outlined, their areal extent in square micrometers was measured, and the labeled cells within the nuclear perimeter were counted. Cellular population densities were expressed as number of cells per 100 μm^2. Their means and standard deviations are listed in Table 1. The population densities of LC1- and S100β-immunoreactive cells from three of the four adult rats with infraorbital nerve transection had been determined in a previous investigation (36). The results from the adult rats surviving 4, 6, and 8 days after cortical ablation were pooled. In order to compare the effects of the lesions, differences in population density between the deprived and the intact side were determined for each nucleus and each animal. The differences were grouped by type and age of lesion and tested for statistical significance with two-tailed, paired *t* tests. Group mean differences are listed in Table 2.

RESULTS

The type of lesion as well as the developmental stage of the brain differentially affected cells immunoreactive for Lipocortin1 (LC1+), phosphotyrosine (PY+), S100β (S100β+), and mannose receptors (MR+). Lipocortin1 was apparent in all resting ramified microglia and showed clear microglial reactions in the stations of the mature whisker-to-barrel pathway deprived by nerve transection or cortical ablation. A fraction of the microglia were immunoreactive for phosphotyrosine; none were immunoreactive for either S100β or mannose receptors. LC1+ microglia of adult morphology were rarely found in newborn rats, and neither type of lesion caused microglial responses in the developing pathway that were of a magnitude comparable to those seen in maturity. Characterization of the cell types responding to the lesions in newborns compared with adults required more detailed scrutiny as described below.

Cell Morphology

Infraorbital nerve transection. In adult rats, LC1+ microglia were omnipresent in the parenchyma of the brain. Infraorbital nerve transection results in a pronounced degeneration of primary afferents terminating in the trigeminal sensory brain-stem nuclei, and LC1+ microglia represented the most conspicuously labeled cell type on the deafferented side. They had polymorphic somata with small (<10 μm) irregularly shaped nuclei and thick cytoplasmic processes with multiple branches (Fig. 1A). Furthermore, PY+ cells were frequently observed on the deafferented side. They possessed polymorphic somata with thick, unbranched, cytoplasmic processes and resembled some of the smaller microglia (Fig. 1B). S100β+ cells were ubiquitous in the brain parenchyma, but did not appear to accumulate on the deafferented side. They had somata with large round nuclei over 10 μm in diameter, typical of astrocytes, and fewer cytoplasmic processes than microglia (Fig. 1C). No changes were observed in the thalamic ventroposterior medial nucleus.

The observations differed considerably in pups 4 days after nerve transection. LC1+ cells were abundant in the ependyma, but sparse in the parenchyma. PY+ cells were also rarely observed. Although infraorbital nerve transection results in the deprivation of afferents to about three-quarters of the territory of the trigeminal sensory brain-stem nuclei, there was no clear, reliable indication that either LC1+ or PY+ cells were increased as a result of the deprivation. In contrast, S100β+ cells were prominent in the parenchyma. They appeared to emanate from the ventricular zone of the fourth ventricle and accumulate on the deprived side. Moreover, the morphology of labeled cells in neonates was distinctly different from that of adults. In contrast to the LC1+ microglia with elongated somata and thick, short processes observed in adults, LC1+ cells in neonates had predominantly obovoid somata with thin, extended cytoplasmic processes (Fig. 1D). While PY+ cells in adults had polymorphic somata, they were pleomorphic in neonates (Fig. 1E). Whereas S100β+ cells in adults had stellate shape and large nuclei, in neonates they had ovoid or fusiform somata, small nuclei, and thin, branching processes (Fig. 1F).

Cortical ablation. The thalamic ventroposterior medial nucleus ipsilateral to cortical ablation is reciprocally connected with the ablated cortex (3, 46) and as a consequence of this type of lesion in adults an abundance of LC1+ cells was observed on the deprived side. They possessed morphological attributes characteristic of activated microglia (Fig. 2A) and bore the greatest resemblance to Forel's spider cells (17). In addition, many PY+ cells were observed. They had small polymorphic somata with thin, ramified processes resembling any of the small microglia (Fig. 2B). Furthermore, S100β+ cells were frequently detected. They had thin processes and somata containing large round nuclei typical of astrocytes (Fig. 2C).

After cortical ablation in neonates, LC1+ cells in the deafferented thalamic ventroposterior medial nucleus had ovoid or spherical somata and were devoid of processes. Many spherical cells bore mitotic figures (Fig. 2D). PY+ cells were either spherical and arborless or pleomorphic with pseudopodia (Fig. 2E). Furthermore, S100β+ cells were either ovoid or spherical (Fig. 2F). The ovoid cells possessed processes and the spherical cells frequently contained toluidine blue-stained granules. Arborless, spherical cells immunoreactive for LC1 and S100β appeared increasingly dense toward the lateral ventricle, suggesting that they may have invaded the parenchyma from the ventricle and successively accumulated at the sites of neural degeneration.

Moreover, distinct differences between adults and neonates in morphology and distribution of labeled cells were observed in parietal cortex near the ablation. In adults, numerous arborless, spherical cells were immunoreactive for LC1 (Fig. 3A). These cells occasionally bore mitotic figures and were well separated from LC1+ microglia found only at a distance from the lesion. A similar segregation was noticed in sections stained for S100β immunoreactivity (Fig. 3B). With few exceptions, S100β+ astrocytes remained outside a zone surrounding the ablation where unlabeled spherical cells were prominent. In neonates as in adults, the only cells immunoreactive for LC1 near the ablation were arborless, spherical cells (Fig. 3C) and such cells were not immunoreactive for S100β (Fig. 3D). However, in neonates S100β+ cells were detected near the ablation. They had darkly stained small polymorphic somata and processes (Fig. 3D).

In contrast to adults, in neonates the spherical cells in parietal cortex permeated the cortical tissue and diminished in density with increasing distance from the boundary of the ablation with the ventricle in harmony with the cell density gradient observed in the thalamus. They expressed mannose receptors (Fig. 3E), suggesting that they were bone marrow-derived macrophages (28, 29) infiltrating the brain parenchyma where the blood–brain barrier was breached. Consistently, spherical MR+ cells were not found where the lesion left the blood–brain barrier intact, i.e., in the deafferented trigeminal sensory brain-stem nuclei. There, the only MR+ cells detected had fusiform somata. They were exclusively situated immediately adjacent to blood vessels (Fig. 3F) and resembled some of the perivascular microglia observed by Linehan *et al.* (29).

Cell Distribution

Infraorbital nerve transection. In both adults and neonates, visible effects of infraorbital nerve tran-

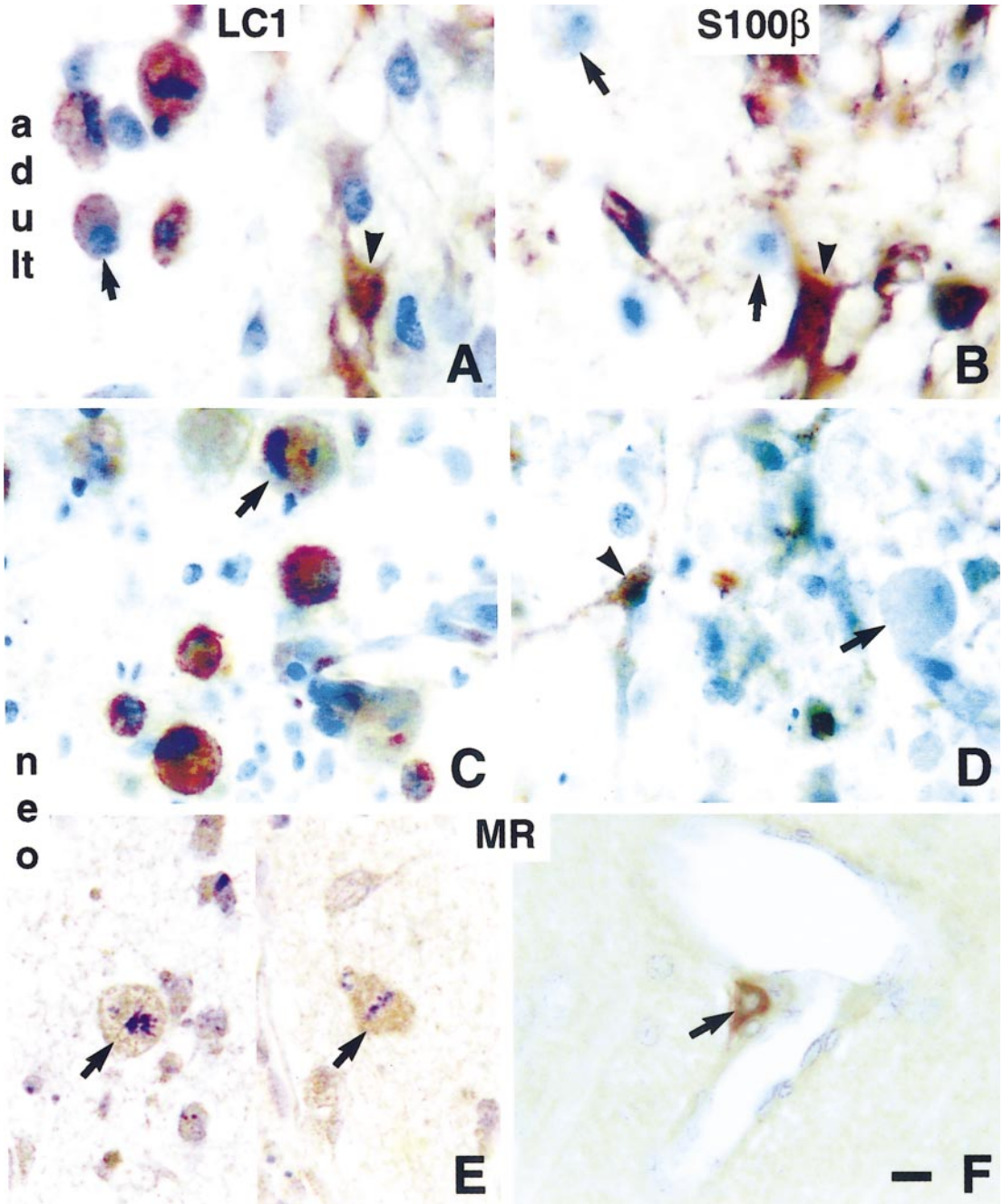

FIG. 3. Cellular responses near the cortical ablation in adults (A and B) and neonates (C, D, and E) 4 days after the ablation. Adjacent 10-μm-thick coronal sections through parietal cortex were processed with immunohistochemistry for LC1 (A and C), S100β (B and D), or MR (E) and stained with toluidine blue. In addition, MR immunoreactivity is shown in a transverse section through deafferented subnucleus caudalis 4 days after neonatal infraorbital nerve transection (F). In adults, immunoreactivity for LC1 was found in microglia (A; arrowhead) and arborless spherical cells (A; arrow) that occasionally bore mitotic figures. The latter resided exclusively within a margin adjacent to the ablation, whereas microglia were found only beyond. A segregation of cells with and without processes was also observed in sections stained for S100β (B). Unstained arborless, spherical cells (B; arrows) were prominent in a zone surrounding the ablation, whereas, with few exceptions, S100β-immunoreactive astrocytes (B; arrowhead) remained outside. In neonates, only arborless, spherical cells immunoreactive for LC1 were found near the ablation (C; arrow). They were most numerous at the boundary of the ablation with the ventricle and diminished in density with increasing distance. In sections stained for S100β, small darkly stained polymorphic cells with processes (D; arrowhead) mingled with large arborless spherical cells lacking immunoreactivity for S100β (D; arrow). The spherical cells were MR immunoreactive (E; arrow), suggesting that they were bone marrow-derived macrophages invading the brain parenchyma through breaches in the blood–brain barrier. In accord, such cells were absent from the brain-stem deafferented by nerve transection where the blood–brain barrier remained intact (F). The only MR+ cell type observed there were vascular pericytes (arrow). Orientation: dorsal is up; the animal's left is on the right. The bar in F represents 10 μm.

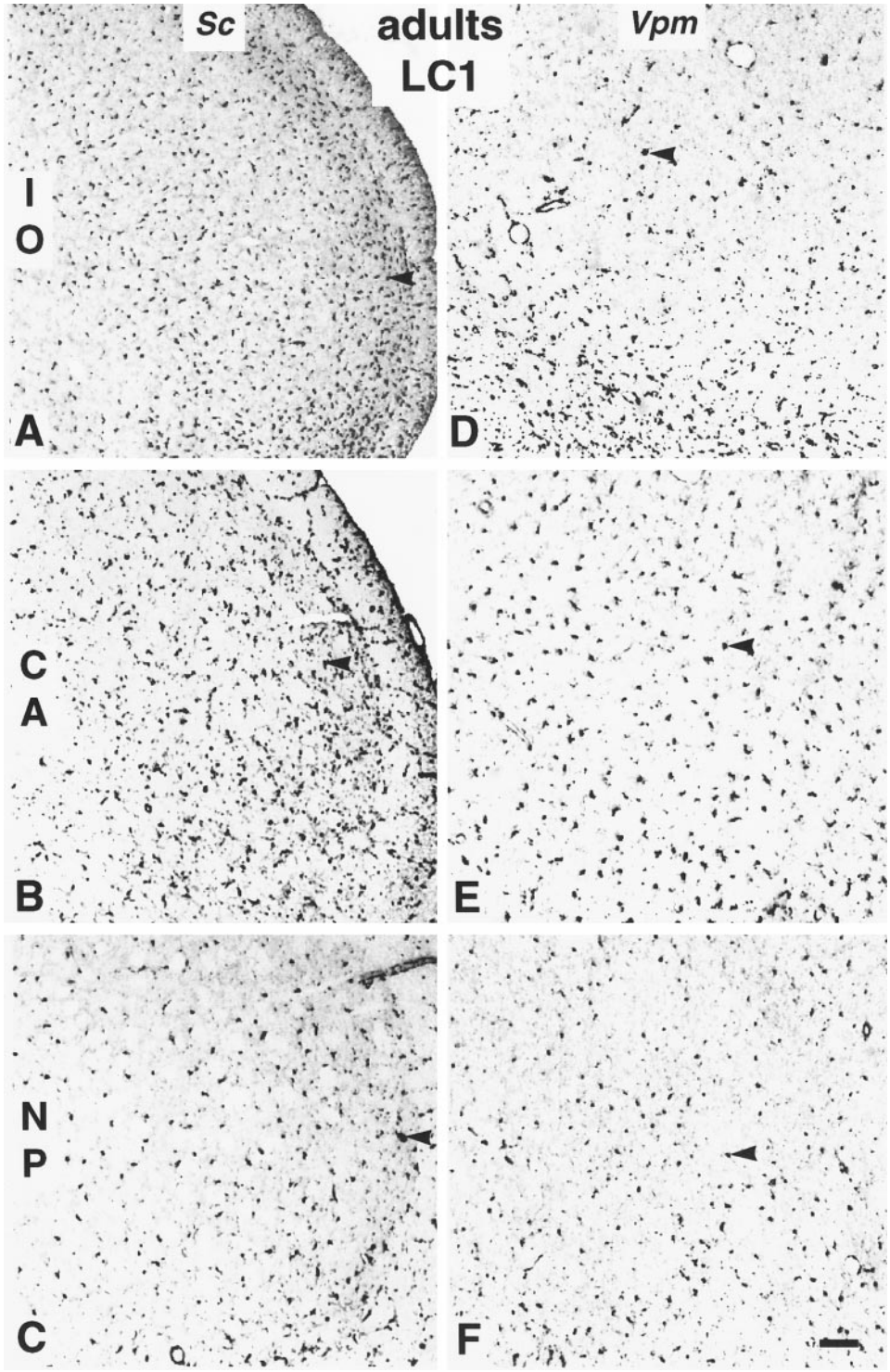

FIG. 4. Effects of the two types of lesion in adults on the distribution of LC1+ microglia in somatic sensory brain-stem and thalamus. Ten-micrometer-thick transverse sections through the subnucleus caudalis Sc (left column) and the thalamic ventroposterior medial nucleus Vpm (right column) were processed with immunohistochemistry for LC1 and stained with toluidine blue 4 days after the lesion. LC1+ cells appear black (arrowheads). The distribution of LC1+ cells on the sides deprived by infraorbital nerve transection (IO; top row) or cortical ablation (CA; middle row) are shown in comparison with the nondeprived, intact side (NP; bottom row). In subnucleus caudalis, LC1+ cells increased on the deprived side after nerve transection (A) and cortical ablation (B) compared with the intact side (C). In the ventroposterior medial nucleus, nerve transection led to a small, hardly noticeable elevation of LC1+ cells (D), whereas cortical ablation resulted in a marked increase (E) compared with the intact side (F). Orientation: dorsal is up; lateral is right in Sc and left in Vpm. To facilitate comparison, the intact sides are reversed about the dorsoventral axis (C, F). The bar in F represents 400 μm.

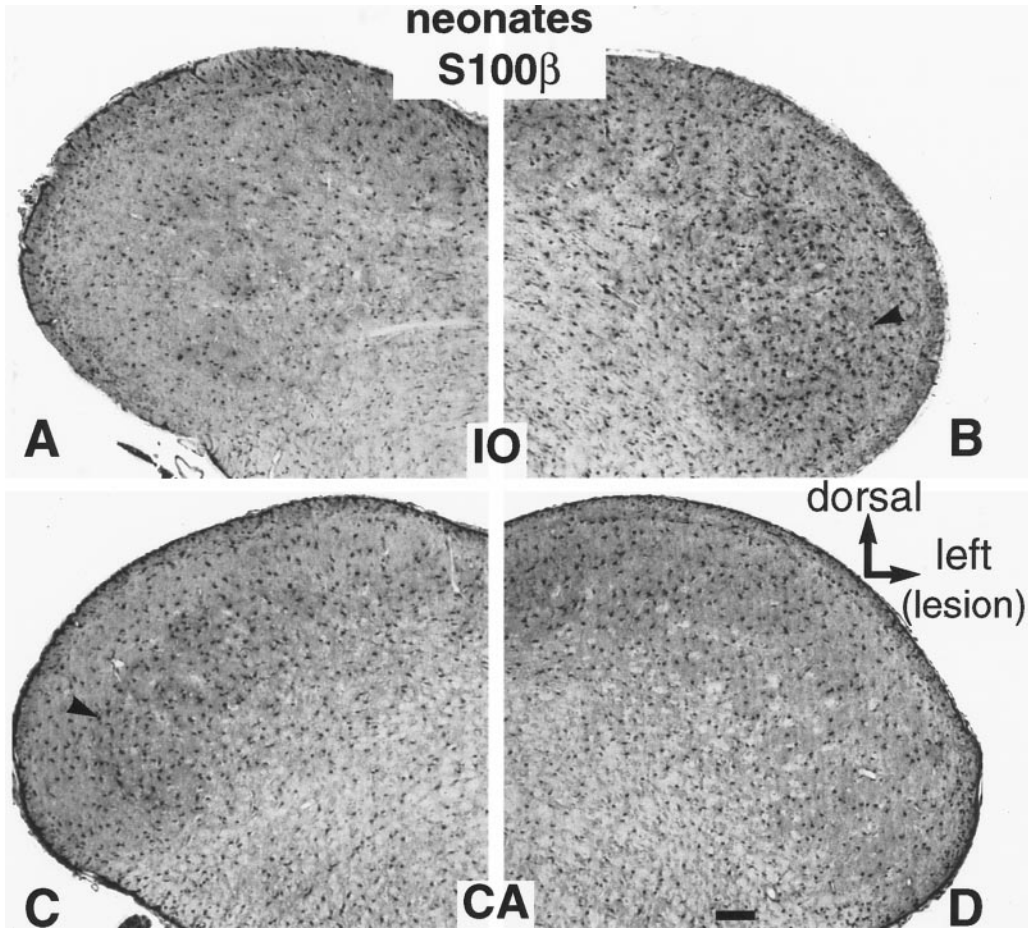

FIG. 5. S100β+ cells in the trigeminal sensory brain-stem of neonates after infraorbital nerve transection (IO; top row) or cortical ablation (CA; bottom row). Ten-micrometer-thick transverse sections through subnucleus caudalis were processed with immunohistochemistry for S100β and stained with toluidine blue 4 days after the lesion. S100β+ cells appear black (arrowheads). Compared with the intact side (A), nerve transection resulted in a distinct increase in S100β+ cells on the deprived side (B). Cortical ablation was less effective, though an increase remained noticeable on the deprived side (C) compared with the intact side (D). Orientation: dorsal is up; the animal's left side is on the right. The bar in D represents 200 μm.

section on the distribution of labeled cells were limited to the trigeminal sensory brain-stem nuclei. In adults, LC1+ cells were clearly more concentrated on the deprived side (compare Figs. 4A and 4C). In neonates, S100β+ cells accumulated there (compare Figs. 5B and 5A). In contrast, in the thalamic ventroposterior medial nucleus, side-to-side differences appeared negligible in both adults (compare Figs. 4D and 4F) and neonates (compare Figs. 6A and 6B).

Cortical ablation. The ascending somatosensory pathway to the ablated cortex originates in the trigeminal sensory brain-stem nuclei contralateral to the ablation (3, 9) and its corticofugal brain-stem connections terminate on that side (46). In accord, after cortical ablations in adults, LC1+ microglia were most visibly increased in the brain-stem nuclei on the side deprived of corticofugal input. Figure 4 shows a clear difference between the deprived (Fig. 4B) and the intact side (Fig. 4C) of subnucleus caudalis. However, cortical ablation seemed to provoke a smaller microglial reaction than infraorbital nerve transection (Fig. 4A). After cortical ablation in neonates, neither LC1+ nor PY+ cells were remarkably increased in the trigeminal sensory brain-stem nuclei. In contrast, S100β+ cells appeared distinctly more concentrated on the deprived side (compare Figs. 5C and 5D). As in adults, the increase seemed smaller than that found after infraorbital nerve transection (Fig. 5B). In the thalamic ventroposterior medial nucleus, cortical ablation in adults resulted in an accumulation of LC1+ cells ipsilateral to the ablation (compare Figs. 4E and 4F). In neonates, however, S100β+ cells accumulated most prominently there (compare Figs. 6C and 6D), whereas LC1+ (compare Figs. 6E and 6F) and PY+ cells (not shown) appeared substantially less increased.

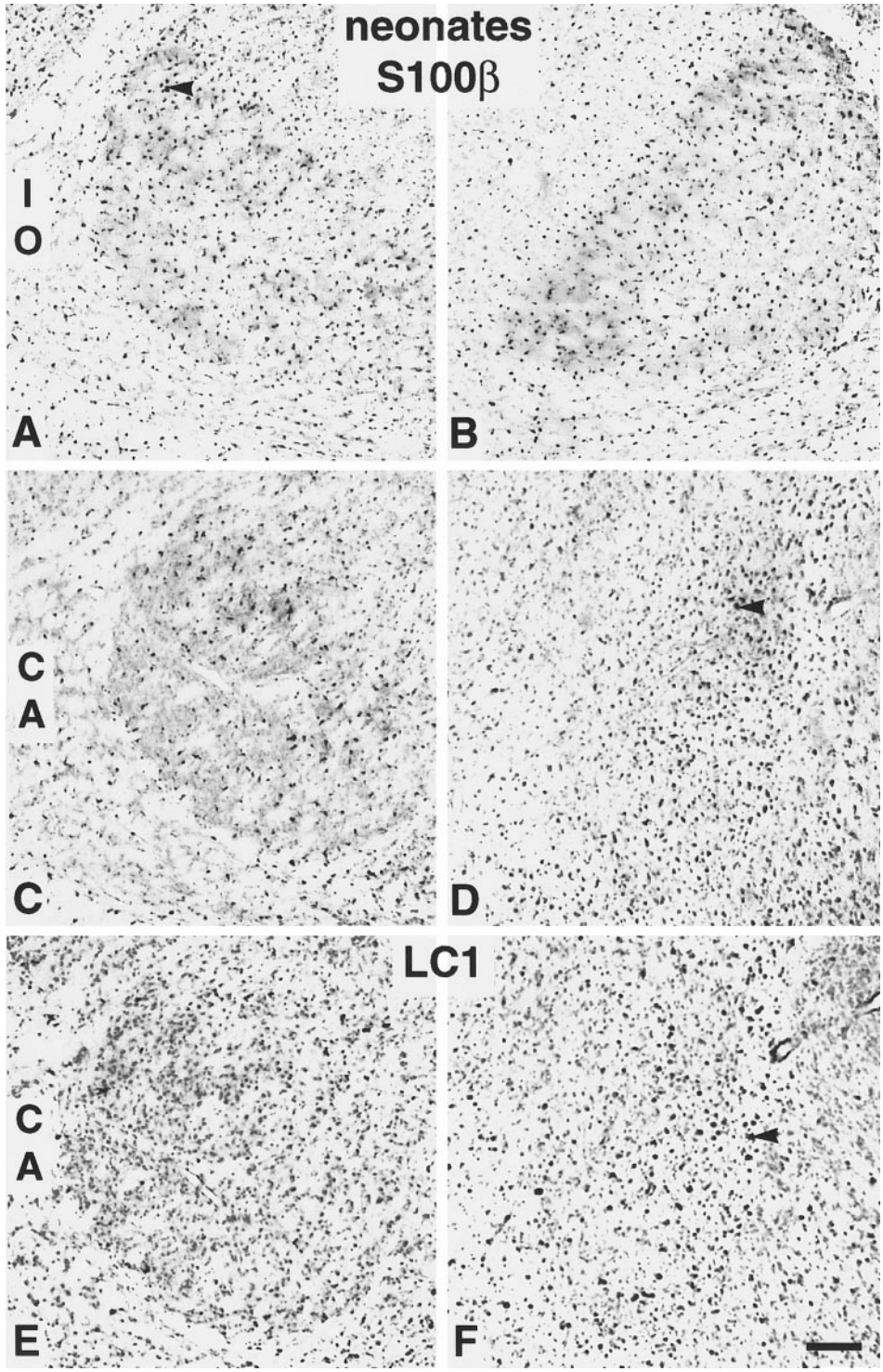

FIG. 6. S100β+ and LC1+ cells in the thalamic ventroposterior medial nucleus after infraorbital nerve transection or cortical ablation in neonates. Ten-micrometer-thick coronal sections through the diencephalon were processed with immunohistochemistry for S100β or LC1 and stained with toluidine blue 4 days after the lesion. S100β+ and LC1+ cells appear black (arrowheads). Nerve transection did not lead to any noticeable increase of S100β+ cells on the deprived side (A) compared with the intact side (B). After cortical ablation, however, S100β+ cells and LC1+ cells were distinctly more numerous on the deprived side (D, F) than on the intact side (C, E). Whereas cortical ablations led to strong deformation of the nucleus (D, F), nerve transection did not have that effect (A). Orientation: dorsal is up; the animal's left is on the right. The bar in F represents 400 μm.

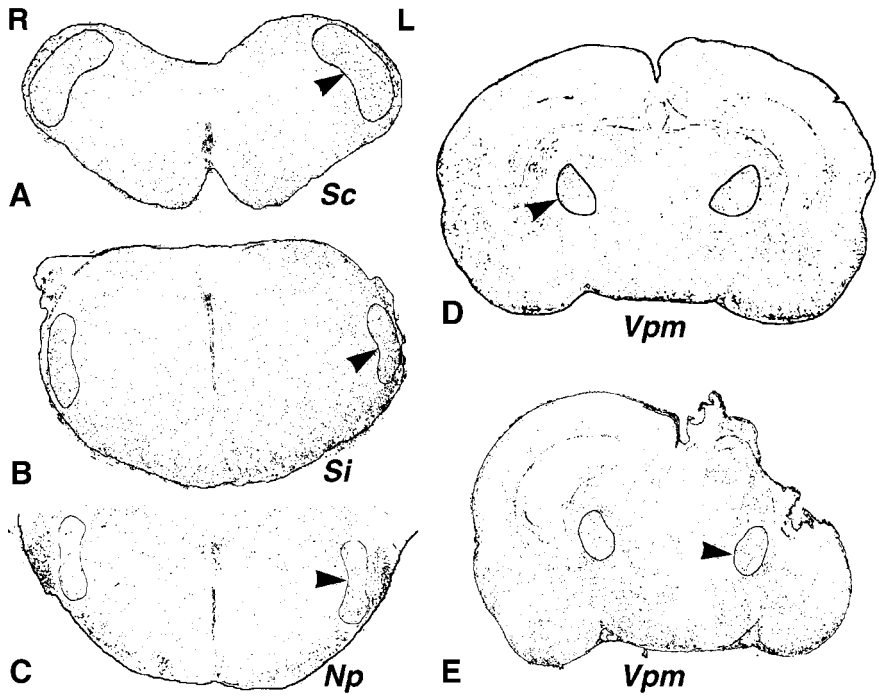

FIG. 7. Typical maps of immunoreactive cellular profiles used to determine cell population densities. The maps show the distribution of S100β+ cells on a transverse section through trigeminal brain-stem subnucleus caudalis Sc (A), subnucleus interpolaris Si (B), and nucleus principalis Np (C) as well as the thalamic ventroposterior medial nucleus Vpm (D) 4 days after infraorbital nerve transection in neonates. In addition, a map from a section through Vpm 4 days after cortical ablation in neonates is shown (E). The boundaries of the sections and the nuclei are outlined. The arrowheads mark the nuclei deprived by the lesions. Marked increases in population density of labeled cells are noticeable in the brain-stem nuclei deafferented by nerve transection and the thalamus deafferented by cortical ablation. In addition, foci of labeled cells can be seen adjacent to blood vessels along the boundaries of the brain-stem. Furthermore, cells in the ependyma and the CSF were frequently labeled (orientation: L—left side of the animal; R—right side of the animal; dorsal is up).

Quantitative Assessment

Figure 7 shows typical maps of immunoreactive cellular profiles in the trigeminal sensory brain-stem nuclei and the thalamic ventroposterior medial nucleus. Such maps were used to determine the population densities in Table 1. In adults, the average population density of LC1+ cells in the intact brain-stem and thalamus was about one cell per 100 μm^2. PY+ cells were substantially fewer. They reached two-thirds of the population density of LC1+ cells. In contrast, the population density of S100β+ cells was three and four times greater than that of LC1+ cells in thalamus and brain-stem, respectively.

In neonates, the population density of LC1+ cells in the intact thalamus and brain-stem was ~20 and ~50% of that in adults, respectively. The population density of PY+ cells was as low as ~10 and ~20%, respectively. In contrast, S100β+ cells were at adult levels in the thalamus and twice as dense as in adults in the brain-stem. Despite the great variability of cell population densities among individuals (Table 1), distinct increases could be observed on the deprived side compared with the intact side, and some reached statistical significance (Table 2).

Infraorbital nerve transection. After nerve transection in adults, PY+ and LC1+ cells in the deprived trigeminal sensory brain-stem increased two- and threefold, respectively (Table 1). The increases were statistically significant at $P \leq 0.01$ (Table 2). Nucleus principalis was most affected (Table 1). Increases in S100β+ cells were smaller than 0.5 cells per 100 μm^2 and remained statistically insignificant (Table 2). After nerve transection in neonates, in contrast, S100β+ cells doubled (Table 1), and this increase was statistically significant (Table 2). The increases in cells immunoreactive for LC1 and PY, however, were insignificant (Table 2). Moreover, increases in cell population density in the deprived thalamic ventroposterior medial nucleus remained insignificant for any marker.

Cortical ablation. After ablation of parietal cortex in adults, LC1+ microglia doubled in the deprived thalamic ventroposterior medial nucleus (Tables 1 and 2). However, this increase reached statistical significance only at $P = 0.10$. Increases in PY+ and S100β+ cells were also observed, but they occurred at lower, even more insignificant levels. In the trigeminal sensory brain-stem nuclei, increases in population density of cells immunoreactive for any marker remained statistically insignificant. Yet, as after nerve transection, brain-stem LC1+ microglia appeared most affected in

TABLE 1

Population Densities of Cells Immunoreactive for Lipocortin1 (LC1), Phosphotyrosine (PY), and S100β in Trigeminal Sensory Brain-Stem Subnucleus Caudalis (Sc), Subnucleus Interpolaris (Si), Nucleus Principalis (Np), and Thalamic Ventroposterior Medial Nucleus (Vpm) after Infraorbital Nerve Transection or Cortical Ablation in Neonates and Adults

		Infraorbital nerve transection cell density (cells/100 μm^2)[a]		Cortical ablation cell density (cells/100 μm^2)[a]	
Station	Age of lesion	Deprived	Nondeprived	Deprived	Nondeprived
LC1					
Sc	Adult	2.61 ± 1.33	0.89 ± 0.34	1.50 ± 0.70	1.04 ± 0.52
	Neonate	0.55 ± 0.34	0.45 ± 0.26	0.90 ± 0.69	0.51 ± 0.41
Si	Adult	3.28 ± 0.19	1.11 ± 0.30	1.06 ± 0.36	0.83 ± 0.21
	Neonate	0.36 ± 0.15	0.32 ± 0.14	0.88 ± 0.70	0.55 ± 0.48
Np	Adult	3.68 ± 0.44	1.26 ± 0.11	1.54 ± 0.75	0.93 ± 0.05
	Neonate	0.71 ± 0.26	0.59 ± 0.21	0.87 ± 0.71	0.45 ± 0.23
Vpm	Adult	0.88 ± 0.33	0.81 ± 0.44	2.70 ± 2.91	0.76 ± 0.31
	Neonate	0.09 ± 0.06	0.07 ± 0.05	0.70 ± 0.19	0.18 ± 0.21
PY					
Sc	Adult	1.75 ± 0.89	0.97 ± 0.35	1.01 ± 0.47	0.70 ± 0.35
	Neonate	0.09 ± 0.03	0.05 ± 0.02	0.40 ± 0.23	0.21 ± 0.19
Si	Adult	2.20 ± 0.13	0.74 ± 0.20	0.71 ± 0.24	0.56 ± 0.14
	Neonate	0.08 ± 0.00	0.03 ± 0.02	0.33 ± 0.11	0.16 ± 0.06
Np	Adult	2.47 ± 0.29	0.84 ± 0.07	1.03 ± 0.50	0.63 ± 0.03
	Neonate	0.12 ± 0.07	0.13 ± 0.10	0.91 ± 0.39	0.34 ± 0.25
Vpm	Adult	0.61 ± 0.19	0.58 ± 0.25	1.39 ± 1.02	0.51 ± 0.21
	Neonate	0.02 ± 0.02	0.01 ± 0.02	0.80 ± 0.31	0.07 ± 0.04
S100β					
Sc	Adult	3.29 ± 0.67	2.92 ± 0.66	5.59 ± 0.80	2.57 ± 0.25
	Neonate	7.09 ± 2.03	4.95 ± 0.72	5.48 ± 0.73	4.27 ± 0.82
Si	Adult	2.21 ± 0.23	1.57 ± 0.43	3.52 ± 0.41	2.48 ± 0.27
	Neonate	5.89 ± 1.90	4.88 ± 0.69	5.33 ± 0.45	4.23 ± 0.48
Np	Adult	3.33 ± 0.68	2.70 ± 0.80	3.96 ± 0.28	2.61 ± 0.35
	Neonate	5.54 ± 1.75	3.87 ± 0.66	5.24 ± 0.97	3.83 ± 0.52
Vpm	Adult	2.76 ± 0.82	2.71 ± 0.35	4.31 ± 0.83	3.02 ± 0.70
	Neonate	3.41 ± 0.93	3.19 ± 0.90	8.66 ± 1.66	2.75 ± 0.29

[a] Means and standard deviations.

nucleus principalis (Table 1). After cortical ablation in neonates, the population density of S100β+ cells in the deprived thalamic ventroposterior medial nucleus increased statistically significantly. The increase was similar to that observed for LC1+ cells in adults with cortical ablations, i.e., about threefold (Table 1). LC1+ and PY+ cells were also elevated. Yet, these increases remained statistically insignificant (Table 2). In harmony with this, S100β+ cells were the only cell type that increased statistically significantly in the trigeminal sensory brain-stem nuclei deprived by cortical ablation (Table 2). The increase was on the average ~25%. As after infraorbital nerve transections, nucleus principalis showed the greatest change (Table 1), i.e., 36%.

DISCUSSION

Infraorbital Nerve Transection

In adult rats, infraorbital nerve transection resulted in a classical microglial reaction in the trigeminal sensory brain-stem nuclei (36). At the second synapse of the whisker-to-barrel pathway, i.e., in the thalamic ventroposterior medial nucleus, the effect was negligible. LC1 and S100β immunoreactivity clearly differentiated microglial from astrocytic populations. In the three brain-stem nuclei examined, LC1+ microglia tripled in population density and exhibited the typical morphological transformation from the resting into the activated state (13). In contrast, the morphology of S100β+ astrocytes did not appear to change and their increase in population density was less than one-tenth of that of microglia. In support of the contention that tyrosine kinases may play a role in the activation of microglia (24), PY immunoreactivity was detected in an increased number of microglia. Not all microglia were PY immunoreactive, however, suggesting that the degree of phosphorylation is spatially and/or temporally regulated.

In neonates infraorbital nerve transection did not result in a typical microglial reaction, though this type of lesion (41) and damage to whisker follicles (42) have

TABLE 2

The Effect of Infraorbital Nerve Transection or Cortical Ablation in Neonates and Adults on Cell Population Densities in the Trigeminal Sensory Brain-Stem and the Thalamic Ventroposterior Medial Nucleus

		Infraorbital nerve transection			Cortical ablation		
		LC1	PY	S100β	LC1	PY	S100β
Station	Age of lesion	Δ cell density (cells/100 mm^2)[a]			Δ cell density (cells/100 mm^2)[a]		
Brain stem	Adult	**2.5**	**1.5**	0.0	0.5	0.5	1.0
	Neonate	0.0	0.0	**1.5**	0.5	0.0	**1.0**
Thalamus	Adult	0.0	0.0	0.0	2.0	1.0	0.5
	Neonate	0.0	0.0	0.0	0.5	0.5	**6.0**

Note. Mean differences in population density of cells immunoreactive for Lipocortin1 (LC1), phosphotyrosine (PY), and S100β between the deprived side and the intact side are given.

[a] Means rounded to the nearest increment of 0.5. Side-to-side differences that were significant at $P \leq 0.01$ in two-tailed paired *t* tests are highlighted in bold.

been demonstrated to lead to considerable reorganization of primary afferents. Cortical barrels develop during the first week after birth and are plastic in response to whisker follicle damage in this critical period. The barrels that would have represented the damaged whisker follicles do not develop and the surrounding barrels enlarge into the vacant territory (14, 23, 25, 45). A similar plasticity has been found in brain stem (5, 10, 14) and thalamus (5, 14), and the morphological changes at the three synaptic relays of the pathway occur concomitant with substantial alterations of functional whisker representations (15, 26, 34, 35). If the microglia in the developing brain were the same as at maturity, this reorganization would result in strong glial activation.

However, neither LC1+ nor PY+ cells in neonates had the features of activated microglia in adults. Their somata were ovoid or pleomorphic and their processes fewer and thinner, resembling the ameboid and pseudopodic microglia that Del Río-Hortega (13) described in the developing brain. Moreover, in neonates neither LC1+ nor PY+ cells changed in population density in response to nerve transection as they do in adults. These findings suggest that either neonatal deafferentiation does not produce the signal that triggers a glial reaction or microglia were too immature to be transformed into the activated state. One important manifestation of this immaturity may consist of the lack of tyrosine phosphorylation.

In contrast to our findings, a microglial reaction has been described in the facial nucleus of newborn rats after the transection of the facial nerve (19). In that study, immunohistochemistry with a polyclonal rabbit antibody against *iba1* (20) was used. This antibody labels resting and activated microglia, but may also stain macrophages (40). Since many cells detected 3 and 5 days after nerve transection also stained for ED1 (19), a large proportion of the cells accumulating in the deprived facial nucleus may have been macrophages. Their appearance may be associated with the prominent hypertrophy and chromatolysis of axotomized motoneurons (6), because in the present study neither macrophages nor chromatolytic perikarya were detected in the trigeminal sensory brain-stem nuclei deafferented by infraorbital nerve transection.

The only cells that distinctly increased in population density in brain-stem and thalamus after infraorbital nerve transection in neonates were S100β immunoreactive. This finding is consistent with the proliferation of astrocytes immunoreactive for glial fibrillary acidic protein (GFAP) in the facial nucleus of neonates after axotomy (19). In the present study, the greatest increase was observed in nucleus principalis in harmony with the findings that after thalamic and cortical lesions in neonates morphological whisker representations do not develop (9, 16) and cell death is most prominent (2, 21) in this nucleus. Interestingly, the S100β+ cells were distinctly dissimilar in morphology and response from astrocytes in adults. They lacked the large round nuclei typical of astrocytes and their population density virtually did not increase after the same type of lesion in adults. Cooper and Steindler (11) showed that immature GFAP-immunoreactive astrocytes outline the boundaries of barrels in parietal cortex before barrels develop and these boundaries were altered following whisker follicle cauterization during the first week after birth. Therefore, immature astrocytes appear to play a crucial role in the development of discrete whisker representations in the whisker-to-barrel pathway. However, future research is needed to elucidate the precise nature of their involvement.

Cortical Ablation

In adult rats, ablation of parietal cortex resulted in the expected glial reaction in the thalamic nuclei where the thalamic radiation originates. In the deprived ventroposterior medial nucleus, LC1+ microglia doubled

in population density and a substantial number of microglia were PY immunoreactive. As after nerve transection, S100β+ astrocytes did not change noticeably in morphology and did not increase statistically significantly in population density. In addition to the thalamic relay, a microglial reaction was observed in the trigeminal sensory brain-stem nuclei contralateral to the ablation. This response may be the result of retrograde degeneration of trigeminothalamic projection neurons owing to the death of their thalamic targets. Nucleus principalis displayed the strongest response, possibly reflecting the fact that the densest trigeminothalamic projection originates in this nucleus (3). Furthermore, the microglial reaction in the brain-stem may be the consequence of anterograde degeneration of corticofugal inputs (46).

In contrast to the activated microglia found in ventroposterior medial nucleus after cortical ablation in adults, LC1+ cells observed in neonates were spherical or ovoid and bare of processes. The ovoid cells matched closely the LC1+ cells observed to emanate from the midline floor-plate raphe (31, 32). The spherical cells bore mitotic figures and resembled the globular forms of microglia that Del Río-Hortega (13) saw specifically in the developing brain. While PY+ cells in adults resembled activated microglia, PY+ cells in neonates were round or pleiomorphic with no resemblance to microglia. Moreover, neonatal S100β+ cells were distinctly different from astrocytes in adults. They were either spherical and bare of processes or fusiform with processes. None had large round nuclei. The fusiform cells were prominent in the brain-stem trigeminal nuclei and appeared similar to astrocytes observed near the paramedian band of the floor plate (30, 31). The spherical cells were found only in thalamus and cortex near the ablation. They often contained toluidine blue-stained granules that may reflect phagocytosis. In adults, astrocytes do not display such granules. Taken together, these differences between neonates and adults are consistent with the contention raised earlier that injured neonatal neurons may not yet be able to trigger a microglial reaction or microglial precursors may still be too undifferentiated to respond. Most likely, the latter possibility applies, because S100β+ cells increased in the trigeminal brain-stem of neonates in response to cortical ablation as well as nerve transection, suggesting the presence of neural signals.

In agreement with the findings of the present study, Milligan *et al.* (37) observed few microglia in newborn rats and an abundance of large, spherical cells in the thalamus after cortical ablation (38). The authors identified these cells as bone marrow-derived macrophages of monocytic origin by differential labeling with antibodies against OX42 and ED1 (37). In accord, in the present study neonatal spherical or pleomorphic LC1+, S100β+, or PY+ cells did not seem to be resident in the brain parenchyma. They were absent from the trigeminal sensory brain-stem nuclei deprived by cortical ablation, though other types of cells labeled by the three markers were present and the population density of S100β+ cells was increased. Rather, they appeared to invade the parenchyma from the ventricle adjacent to the ablation and accumulate in the deprived thalamus underneath. Consistent with this interpretation, spherical cells near the ablation were immunoreactive for mannose receptors specific to blood-borne macrophages (29) and such cells were not found in the brain-stem. Our findings and those of Milligan *et al.* (37, 38), thus, disagree with the notion that macrophages are precursors of microglia (12). Intriguingly, the entry of spherical cells into the cerebral parenchyma at the site of the cortical ablation appears to be blocked in adults. The glial reaction in the mature brain may, therefore, have suppressed the infiltration of bone marrow-derived macrophages into the brain tissue though the blood–brain barrier was disrupted. In harmony with this notion, LC1 has been observed to suppress the recruitment of macrophages (18).

The absence of macrophages in the deprived neonatal brain-stem nuclei after cortical ablation or nerve transection suggests that it is unlikely that macrophages serve as substitutes for phagocytic microglia during normal brain development. Instead, they may assume such function only after the blood–brain barrier has been broken and their range is limited to the vicinity of the break as cortical ablation demonstrates. Therefore, the question remains to be answered which cells fulfill the role of microglia as scavengers of neuronal debris in a phase of development when the brain is most plastic and pathways are shaped by exuberance and elimination of neuronal connections and apoptosis.

ACKNOWLEDGMENTS

We are indebted to Professors N. G. Ahn, University of Colorado (Boulder, CO), L. J. Van Eldik, Northwestern University (Chicago, IL), and V. L. Shepherd, Vanderbilt University (Nashville, TN), for providing us with antibodies for Lipocortin1, S100β, and mannose receptors, respectively.

REFERENCES

1. Arvidsson, J. 1986. Transganglionic degeneration in vibrissae innervating primary sensory neurons of the rat: A light and electron microscopic study. *J. Comp. Neurol.* **249:** 392–403.
2. Ashwell, K. W. S., and P. M. E. Waite. 1991. Cell death in the developing trigeminal nuclear complex of the rat. *Dev. Brain Res.* **63:** 291–295.
3. Bates, C. A., and H. P. Killackey. 1985. The organization of the neonatal rat's brainstem trigeminal complex and its role in the formation of central trigeminal patterns. *J. Comp. Neurol.* **240:** 265–287.
4. Belford, G. R., and H. P. Killackey. 1979. Vibrissae representation in subcortical trigeminal centers of the neonatal rat. *J. Comp. Neurol.* **183:** 305–322.

5. Belford, G. R., and H. P. Killackey. 1980. The sensitive period in the development of the trigeminal system of the neonatal rat. *J. Comp. Neurol.* **193:** 335–350.
6. Bodian, D., and R. C. Mellors. 1945. The regenerative cycle of motoneurons with special reference to phosphatase activity. *J. Exp. Med.* **81:** 469–488.
7. Cammermeyer, J. 1965. Juxtavascular karyokinesis and microglia cell proliferation during retrograde reaction in the mouse facial nucleus. *Ergeb. Anat. Entwickl.-Gesch.* **38:** 1–22.
8. Catalano, S. M., R. T. Robertson, and H. P. Killackey. 1995. Rapid alteration of thalamocortical axon morphology follows peripheral damage in the neonatal rat. *Proc. Natl. Acad. Sci. USA* **92:** 2549–2552.
9. Chiaia, N. L., C. A. Bennett-Clarke, and R. W. Rhoades. 1991. Effects of cortical and thalamic lesions upon primary afferent terminations, distributions of projection neurons, and the cytochrome oxidase pattern in the trigeminal brainstem complex. *J. Comp. Neurol.* **303:** 600–616.
10. Chiaia, N. L., C. A. Bennett-Clarke, M. Eck, F. A. White, R. S. Crissman, and R. W. Rhoades. 1992. Evidence for prenatal competition among the central arbors of trigeminal primary afferent neurons. *J. Neurosci.* **12:** 62–76.
11. Cooper, N. G. F., and D. A. Steindler. 1989. Critical period-dependent alterations of the transient body image in the rodent cerebral cortex. *Brain Res.* **489:** 167–176.
12. Dalmau, I., B. Finsen, N. Tønder, J. Zimmer, B. Gonzáles, and B. Castellano. 1997. Development of microglia in the prenatal rat hippocampus. *J. Comp. Neurol.* **377:** 70–84.
13. Del Río-Hortega, P. 1932. Microglia. Pages 481–534 in W. Penfield, Ed., *Cytology and Cellular Pathology of the Nervous System,* Vol. 2. Hoeber, New York.
14. Durham, D., and T. A. Woolsey. 1984. Effects of neonatal whisker lesions on mouse central trigeminal pathway. *J. Comp. Neurol.* **223:** 424–447.
15. Durham, D., and T. A. Woolsey. 1985. Functional organization in cortical barrels of normal and vibrissae-damaged mice: A [^{3}H]2-deoxyglucose study. *J. Comp. Neurol.* **235:** 97–110.
16. Erzurumlu, R. S., and F. F. Ebner. 1988. Maintenance of discrete somatosensory maps in subcortical relay nuclei is dependent on an intact sensory cortex. *Dev. Brain Res.* **44:** 302–308.
17. Forel, A. 1907. Pages 170–176 in *Gesammelte hirnanatomische Abhandlungen mit einem Aufsatz über die Aufgaben der Neurobiologie.* Reinhardt, Munich.
18. Getting, S. J., R. J. Flower, and M. Perretti. 1997. Inhibition of neutrophil and monocyte recruitment by endogenous and exogenous lipocortin 1. *Br. J. Pharmacol.* **120:** 1075–1082.
19. Graeber, M. B., F. López-Redondo, E. Ikoma, M. Ishikawa, Y. Imai, K. Nakajiama, G. W. Kreutzberg, and S. Kohasaka. 1998. The microglia/macrophage response in the neonatal rat facial nucleus following axotomy. *Brain Res.* **813:** 241–253.
20. Imai, Y., I. Ibata, D. Ito, K. Ohsawa, and S. Kohsaka. 1996. A novel gene *iba1* in the major histocompatibility complex class III region encoding an EF hand protein expressed in a monocytic lineage. *Biochem. Biophys. Res. Commun.* **224:** 855–862.
21. Jacquin, M. F., J. Z. Rana, M. W. Miller, and N. L. Chiaia. 1996. Development of trigeminal nucleus principalis in the rat—Effect of target removal at birth. *Eur. J. Neurosci.* **8:** 1641–1657.
22. Jacquin, M. F., W. E. Renehan, B. G. Klein, R. D. Mooney, and R. W. Rhoades. 1986. Functional consequences of neonatal infraorbital nerve section in rat trigeminal ganglion. *J. Neurosci.* **6:** 3706–3720.
23. Jeanmonod, D., F. L. Rice, and H. Van der Loos. 1981. Mouse somatosensory cortex: Alterations in the barrelfield following receptor injury at different early postnatal ages. *Neuroscience* **6:** 1503–1535.
24. Karp, H. L., M. L. Tillotson, J. Soria, C. Reich, and J. G. Wood. 1994. Microglial tyrosine phosphorylation systems in normal and degenerating brain. *Glia* **11:** 284–290.
25. Killackey, H. P., and G. R. Belford. 1979. The formation of afferent patterns in the somatosensory cortex of the neonatal rat. *J. Comp. Neurol.* **183:** 285–304.
26. Kossut, M., and P. Hand. 1984. Early development of changes in cortical representation of C3 vibrissa following neonatal denervation of surrounding vibrissa receptors: A 2-deoxyglucose study in the rat. *Neurosci. Lett.* **46:** 7–12.
27. Kreutzberg, G. W. 1966. Autoradiographische Untersuchungen über die Beteiligung von Gliazellen an der axonalen Reaktion im Facialiskern der Ratte. *Acta Neuropathol. (Berlin)* **7:** 149–161.
28. Lennartz, M. R., F. S. Cole, V. L. Shepherd, T. E. Wileman, and P. D. Stahl. 1987. Isolation and characterization of a mannose-specific endocytosis receptor from human placenta. *J. Biol. Chem.* **262:** 9942–9944.
29. Linehan, S. A., L. Martínez-Pomares, P. D. Stahl, and S. Gordon. 1999. Mannose receptor and its putative ligands in normal murine lymphoid and nonlymphoid organs: In situ expression of mannose receptor by selected macrophages, endothelial cells, perivascular microglia, and mesangial cells, but not dendritic cells. *J. Exp. Med.* **189:** 1961–1972.
30. Ma, P., and T. A. Woolsey. 1984. Cytoarchitectonic correlates of the vibrissae in the medullary trigeminal complex of the mouse. *Brain Res.* **306:** 374–379.
31. McKanna, J. A. 1993. Lipocortin1 immunoreactivity identifies microglia in adult rat brain. *J. Neurosci. Res.* **36:** 491–500.
32. McKanna, J. A., and S. Federoff. 1996. Development of microglia *in situ* and in culture. Pages 21–42 in E. A. Ling, C. K. Tan, and C. B. C. Tan, Eds., *Topical Issues in Microglia Research.* Singapore Neurosci. Assoc., Goh Bros. Enterprise Humanities Press, Singapore.
33. McKanna, J. A., and M.-Z. Zhang. 1997. Immunohistochemical localization of lipocortin 1 in rat brain is sensitive to pH, freezing, and dehydration. *J. Histochem. Cytochem.* **45:** 527–538.
34. Melzer, P., A. M. Crane, and C. B. Smith. 1993. Mouse barrel cortex functionally compensates for deprivation produced by neonatal lesion of whisker follicles. *Eur. J. Neurosci.* **5:** 1638–1652.
35. Melzer, P., and C. B. Smith. 1996. Plasticity of metabolic whisker maps in somatosensory brainstem and thalamus of mice with neonatal lesions of whisker follicles. *Eur. J. Neurosci.* **8:** 1853–1864.
36. Melzer, P., M.-Z. Zhang, and J. A. McKanna. 1997. Infraorbital nerve transection and whisker follicle removal in adult rats affect microglia and astrocytes in the trigeminal brainstem. A study with Lipocortin1- and S100β-immunohistochemistry. *Neuroscience* **80:** 459–472.
37. Milligan, C. A., T. J. Cunningham, and P. Levitt. 1991. Differential immunochemical markers reveal the normal distribution of brain macrophages and microglia in the developing rat brain. *J. Comp. Neurol.* **314:** 125–135.
38. Milligan, C. A., P. Levitt, and T. J. Cunningham. 1991. Brain macrophages and microglia respond differently to lesions of the developing and adult visual system. *J. Comp. Neurol.* **314:** 136–146.
39. Penfield, W. 1925. Microglia and the process of phagocytosis in gliomas. *J. Pathol.* **1:** 77.
40. Reivich, G., L. L. Jones, C. U. A. Kloss, A. Werner, H. Neumann, and G. W. Kreutzberg. 1998. Immune surveillance in the injured nervous system: T-lymphocytes invade the axotomized mouse facial motor nucleus and aggregate around sites of neuronal degeneration. *J. Neurosci.* **18:** 5804–5816.

41. Renehan, W. E., R. W. Rhoades, and M. F. Jacquin. 1989. Structure–function relationships in rat brainstem subnucleus interpolaris. VII. Primary afferent central terminal arbors in adults subjected to infraorbital nerve section at birth. *J. Comp. Neurol.* **289:** 493–508.

42. Renehan, W. E., R. S. Crissman, and M. F. Jacquin. 1994. Primary afferent plasticity following partial denervation of the trigeminal brainstem nuclear complex in the postnatal rat. *J. Neurosci.* **14:** 721–739.

43. Streit, W. J., and G. W. Kreutzberg. 1988. Response of endogenous glial cells to motor neuron degeneration induced by toxic ricin. *J. Comp. Neurol.* **268:** 248–263.

44. Van der Loos, H. 1976. Barreloids in mouse somatosensory thalamus. *Neurosci. Lett.* **2:** 1–6.

45. Van der Loos, H., and T. A. Woolsey. 1973. Somatosensory cortex: Structural alterations following early injury to sense organs. *Science* **179:** 395–397.

46. Welker, E., P. V. Hoogland, and H. Van der Loos. 1988. Organization of feedback and feedforward projections of the barrel cortex: A PHA-L study in the mouse. *Exp. Brain Res.* **73:** 411–435.

47. Woolsey, T. A., and H. Van der Loos. 1970. The structural organization of layer IV in the somatosensory region (SMI) of mouse cerebral cortex. The description of a cortical field composed of discrete cytoarchitectonic units. *Brain Res.* **17:** 205–242.